AIP Advances

Synthesis of β-Ga_2O_3 thin film assisted by microwave annealing

Cite as: AIP Advances **12**, 085118 (2022); https://doi.org/10.1063/5.0110530
Submitted: 16 July 2022 • Accepted: 05 August 2022 • Published Online: 23 August 2022

Nafiseh Badiei, Afshin Tarat and Lijie Li

COLLECTIONS

This paper was selected as Featured

AIP Advances
Mathematical Physics Collection
READ NOW

© 2022 Author(s).

Synthesis of β-Ga_2O_3 thin film assisted by microwave annealing

Cite as: AIP Advances 12, 085118 (2022); doi: 10.1063/5.0110530
Submitted: 16 July 2022 • Accepted: 5 August 2022 •
Published Online: 23 August 2022

View Online

Export Citation

CrossMark

Nafiseh Badiei, Afshin Tarat, and Lijie Li[a)]

AFFILIATIONS

College of Engineering, Swansea University, Swansea SA1 8EN, United Kingdom

[a)]Author to whom correspondence should be addressed: L.Li@swansea.ac.uk

ABSTRACT

β-Ga_2O_3 is increasingly being used in power electronics and UV sensors. The preparation of β-Ga_2O_3 thin films requires costly and time-consuming fabrication processes. Therefore, developing short-time and low-cost fabrication processes of the β-Ga_2O_3 thin film has been greatly demanded to quicken the pace of applying this material in practical devices and systems. In this paper, a new fabrication process combining physical vapor deposition and microwave localized annealing has been postulated for β-Ga_2O_3 thin films. The experimental results show that after microwave annealing bandgaps have been slightly adjusted, the surface morphology has been improved and extra diffraction peaks appear, which give rise to stronger β-phase characteristics in the Ga_2O_3 thin film. Calculation based on density functional theory has been conducted to show the electronic bandstructures, formation energies, and optical absorptions of both types.

© 2022 Author(s). All article content, except where otherwise noted, is licensed under a Creative Commons Attribution (CC BY) license (http://creativecommons.org/licenses/by/4.0/). https://doi.org/10.1063/5.0110530

INTRODUCTION

Gallium oxide (Ga_2O_3) has attracted great attention for its unique semiconductor properties, such as a wide direct bandgap of 4.5–4.9 eV and a large breakdown field strength (8 MV/cm), which offers promising applications in optoelectronic and power electronic devices and systems.[1] Ga_2O_3 is a polymorphic compound with different crystalline phases (α, β, γ, δ, and ε); in addition, a transient κ-Ga_2O_3 polymorph has been reported.[2] Beta-phase gallium oxide (β-Ga_2O_3) is regarded as the most thermodynamically stable phase out of its five existing phases.[1] Devices built upon β-Ga_2O_3 have promising applications in power electronics,[3] LEDs,[4] and solar-blind photodetectors.[5,6] Vertical and lateral transistors based on β-Ga_2O_3 have been fabricated to demonstrate the feasibility of applying this material in power electronics.[7,8] The two-dimensional (2D) Ga_2O_3 has been investigated theoretically due to the potential improvements in tunable bandgap by strain and high surface-area-to-volume ratio against its bulk form. Several theoretical studies have been conducted on 2D Ga_2O_3 to investigate its electronic and optical properties.[9,10] Among these crystalline phases, different fabrication techniques and characterization of the α- and β- Ga_2O_3 have been conducted.[11] Phase transitions among these phases have also been reported using the thermal annealing technique, namely, κ-Ga_2O_3 to β-Ga_2O_3,[12] α-phase to β-phase at elevated temperature,[13] and reverse transition from β to α.[14] The β-crystal is the most common and well-studied polymorph of gallium oxide and is the only stable crystal at different temperatures until the melting point at 1900 °C. In addition, the studies confirmed that all other crystal forms show a metastable property and transform into β-crystal structure at a temperature of over 700 °C. This thermal stability makes it possible to fabricate either a single crystal or uniform thin films via a high temperature process such as crystallization from a melt or vapor phase epitaxy. Along with other methods, different microwave-assisted techniques have been successfully used to synthesize various gallium oxide hydroxide (α-GaOOH) nanorods and nanocrystal structures.[15] The thermal decomposition of 60 min α-GaOOH at 600 °C in the air for 4 h results in Ga_2O_3 nanostructures crystalline micrometer/submicron-nanorods.[16] The microwave (MW) irradiation treatment method is a fast, precise, non-contact technology that can induce changes in morphological, chemical, optical, and structural properties during irradiation treatment.[17–19] Moreover, localized phase changing can be realized based on patterned substrates. When the materials are irradiated by MWs, which have low frequency with low energy, they are hardly damaged. Thus, MW irradiation can be non-destructive and more economical compared to other irradiation treatment methods such as UV radiation, gamma rays, and ion beams. Furthermore, MWs can heat wafers in localized regions

compared to conventional annealing because energy can be delivered by radiation rather than by conduction or convection. Ultimately, commercial microwave ovens are easily accessible. In this study, for the first time, MW irradiation, in combination with the physical vapor deposition technique, was successfully used to synthesize β-Ga_2O_3.

EXPERIMENTAL METHOD

Two substrates [100-nm-thick n-type Si and fused silica UV grade quartz substrates (Inseto Limited)] were prepared to deposit Ga_2O_3 thin films. The substrates (four samples of each substrate) were cleaned by ultra-sonication, with the following cleaning sequence: acetone–Isopropanol–deionized (DI) water; then, the samples were fully dried using a nitrogen gun and were subsequently heated at 180 °C for 10 min on a hotplate to be completely dehydrated. Then, 300 nm Ga_2O_3 thin films were deposited onto the substrates (Inseto Limited) by radio-frequency (RF) magnetron sputtering (PVD) at room temperature. As-fabricated samples were treated using a commercial kitchen microwave oven (KENWOOD, Model: K30CSS14, 900 W, 2.45 GHz). The samples were treated for 5, 10, and 20 min and prepared for characterization. For comparison purpose, the samples were synthesized with traditional PVD and furnace annealing; the furnace annealing temperature and time were 700 °C and 40 min, respectively.

MATERIAL CHARACTERIZATION AND SIMULATION

Figure 1(a) illustrates the schematic representation of crystal structures of α- and β-phase Ga_2O_3. The space group of α-Ga_2O_3 is R-3c and that of β-Ga_2O_3 is C2/m. It is worth mentioning that, in this experiment, the α-Ga_2O_3 is amorphous as it was grown by PVD at room temperature and the target used in the PVD was amorphous Ga_2O_3. X-ray diffraction (XRD) is a non-destructive analysis technique used to identify the crystalline structure and phases present in a material and thereby reveal the chemical composition information. The XRD (Bruker D8 Advance x-ray diffractometer) results of the deposited films along with n-type Si substrate are shown in Fig. 1(b). The peaks at ~64.4° and ~77.4° correspond to forbidden (512) and (421) plane reflections, respectively.[20,21] Those are well attributed to the monoclinic β-phase Ga_2O_3. The intensity of these peaks is nearly undetectable in non-MW treated sample to the highest intensity in 20 min MW treated one. In Fig. 1(b), subplots (i)–(v) are as-grown, 5, 10, 20 min microwave treated, and using the traditional furnace annealing, respectively. It is clearly shown in Fig. 1(b) that there are many changes in the XRD peaks from as-grown to 5 min MW treatment. For example, peaks at 32.8°, 51.1°, 55.4°, 59.9°, 63.2°, and 65.4° have disappeared, and peaks at 38°, 44.2°, 64.4°, and 77.4° have emerged, reflecting the phase change. It is envisaged that heating on the wafer by the microwave energy anneals the sample, causing phase change from α to β. Further experiments will be conducted for device applications.

Transmittance measurements of α-Ga_2O_3 (amorphous) and microwave irradiated (crystalline) Ga_2O_3 thin films were performed on a double-beam UV/Vis/NIR (Perkin-Elmer Lambda 9 spectrophotometer). A β-Ga_2O_3 film grown by the PVD with post annealing process within a furnace has demonstrated a bandgap of

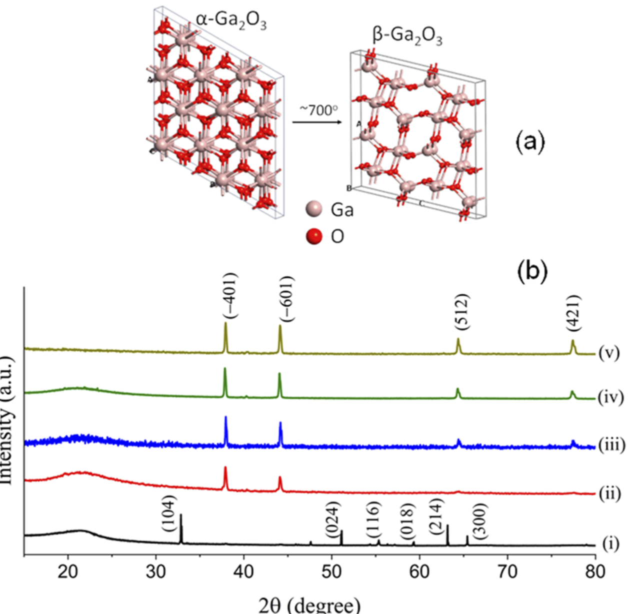

FIG. 1. (a) Schematic representation of crystal structures for α- and β-phase Ga_2O_3. (b) XRD measurement of as-grown (i), 5 min (ii), 10 min (iii), 20 min microwave treatment (iv), and β-Ga_2O_3 made using traditional furnace annealing (v).

4.65 eV [for comparison, see the Tauc plot shown in Fig. 2(a)]. By examining the Tauc plots [Fig. 2(b)] of the MW treated samples, it is shown that the bandgaps of the material are 4.9, 4.8, and 4.75 eV for as-grown from room temperature PVD, 5 min MW treatment, and 20 min MW treatment, respectively. The results display a clear bandgap reduction trend with an increase in the MW treatment time. This aspect potentially reflects that the MW can be a low-cost annealing method to change the crystalline phase from alpha to beta. The XRD and UV–Vis results show a phase change from alpha to beta during microwave treatments; therefore, according to the previous papers, it is estimated that the localized heating on the sample in the microwave unit should be at least 600–700 °C. It was reported previously for the furnace annealing[22] that N_2 annealing is better as it helps to improve the crystallinity of Ga_2O_3 and in the passivation of dangling bonds related to oxygen defects at grain boundaries. The kitchen microwave oven used in this work does not have any control on annealing the samples with any gas such as N_2 or O_2. It is expected that a controlled ambient gas (N_2 or O_2) during the microwave annealing will make a similar difference as with furnace annealing.

SEM (Hitachi 4800 S) was used to image the 300 nm thick Ga_2O_3 samples before and after 5 and 20 min MW treatments. With an increase in the MW treatment time, evidence of particle agglomeration, annealing, and sintering begin to be observed. Figure 3(a) shows the sample before MW treatment. After 5 min MW treatment [Fig. 3(b)], samples begin to exhibit annealing and sintering effects, and further annealing can be seen after 20 min MW treatment [Fig. 3(c)].

© Author(s) 2022

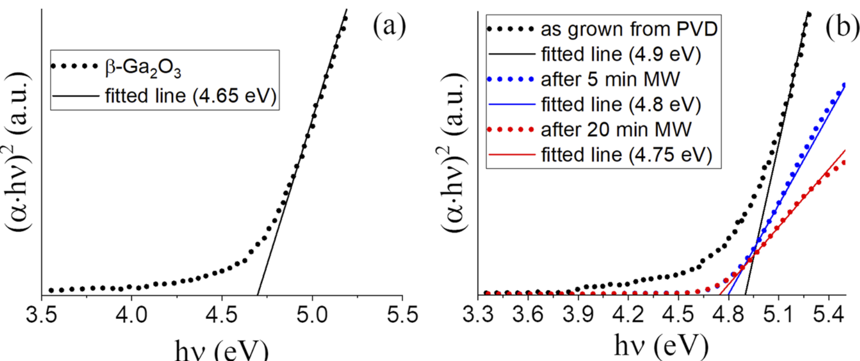

FIG. 2. (a) Tauc plot of β-Ga_2O_3 prepared with traditional PVD plus furnace annealing. (b) Tauc plots for microwave treated Ga_2O_3 thin films.

Density functional theory (DFT) simulation has been performed using the QuantumATK software to better understand the difference between α-Ga_2O_3 and β-Ga_2O_3 in terms of their electronic and optical properties. Both supercells of these two crystalline types have been built and subsequently geometrically optimized. The α-Ga_2O_3 supercell is hexagonal (corundum-like structure, similar to Al_2O_3), contains 12 Ga and 18 O, and the space group belongs to R-3c. The geometrical optimization was made using the exchange correlation of generalized gradient approximation (GGA) and the Perdew–Burke–Ernzerhof (PBE) predefined functional. The density mesh cut off was made to 125 Hartree, and k-point sampling was $7 \times 7 \times 2$. During the optimization process, the maximum force tolerance was 0.01 eV/Å and the maximum stress tolerance was 0.001 eV/Å^3. The optimized supercell has the lattice parameters as follows: $a = b = 5.07$ Å; $c = 13.62$ Å; $\alpha = 90°$; $\beta = 90°$; $\gamma = 120°$; Volume = 303.47 Å^3. The same geometrical optimization procedure was used to optimize β-Ga_2O_3, whose supercell is monoclinic, and has 8 Ga and 12 O. The exchange correlation and predefined functionals are the same as used in the α-Ga_2O_3 optimization process except the k-point sampling, which was $3 \times 9 \times 5$ for β-Ga_2O_3. The optimized β-Ga_2O_3 has the following lattice parameters: $a = 12.42$ Å; $b = 3.09$ Å; $c = 5.89$ Å; $\beta = 103.64°$; Volume = 219.46 Å^3. After geometrical optimization, the electronic and optical properties of these two phase types have been calculated. In the property calculations, a more accurate algorithm (Meta-GGA) has been used, as the PBE functional usually leads to the underestimation of bandgaps.[23] In the simulation, the exchange correlation is MGGA with c parameter set to 1.37. The exchange functional of TB09 was used, the density mesh cut off value was 80 Hartree, the broadening was set to 0.1 eV, and the

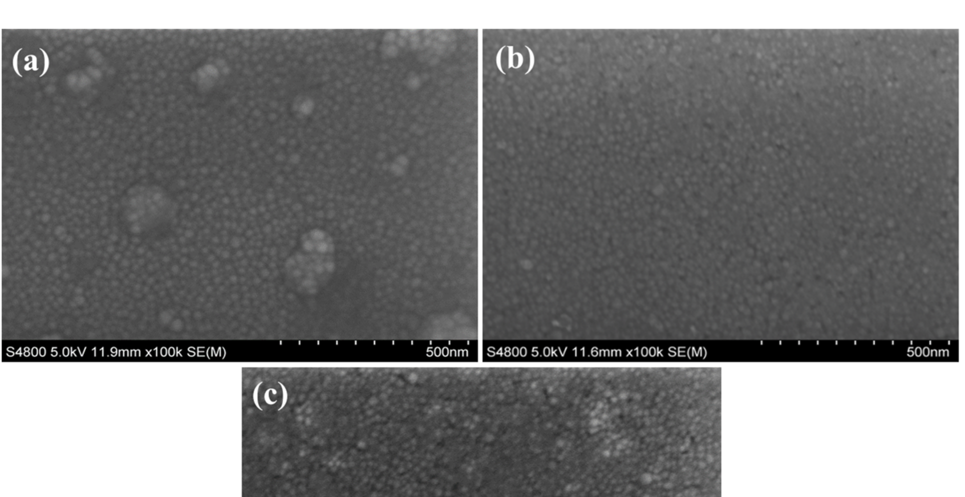

FIG. 3. SEM images of 300 nm thick Ga_2O_3 not treated (a), 5 min MW treated (b), and 20 min MW treated (c).

© Author(s) 2022

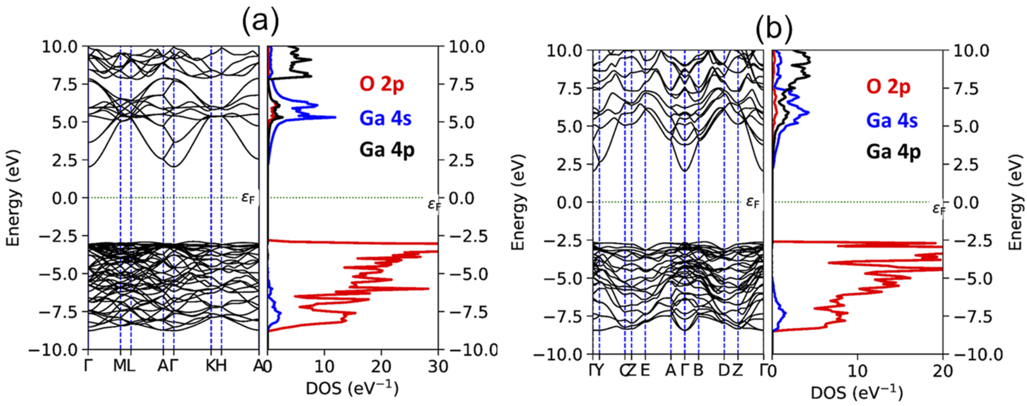

FIG. 4. Bandstructures and density of states of α-Ga_2O_3 (a) and β-Ga_2O_3 (b).

k-point samplings for both have been the same as in the geometrical optimizations.

It is seen from the DFT simulation results in Fig. 4 that the direct bandgaps of the α-Ga_2O_3 and β-Ga_2O_3 are 5.21 and 4.82 eV, respectively. The bandgap of corundum-like α-Ga_2O_3 has been measured to be in the range of 4.9–5.6 eV,[24–26] which matches well with the DFT simulation results in this work. It is also found from the density of states (DOS) plots that the valence bands for both types are pretty much similar (both are dominated by electrons on the O 2p orbital) except that the effective mass of β-Ga_2O_3 appears slightly smaller than that of α-Ga_2O_3, which coincides with the experimental results shown in Fig. 2. The DFT simulation has validated that there are phase changes facilitated by the low-cost microwave treatments. In the experiment, the bandgap underwent reductions from 4.9 eV down to 4.75 eV after 20 min of microwave radiation. The bandgap value of 4.75 eV is very much close to the β-Ga_2O_3 [4.65 eV in Fig. 2(a)] obtained by the time-consuming furnace annealing process. A major difference can be found in conduction bands from Fig. 4. For example, the DOS of Ga 4 s has a clearer peak and is much stronger in α-Ga_2O_3 than that in β-Ga_2O_3. Moreover, a slightly wider bandgap of the α-Ga_2O_3 indicates that there is a potential application for α-Ga_2O_3 to be used in far UV devices. Inspired by the bandstructure results, further DFT studies have been conducted on the optical absorption spectra of both crystal types. The same simulation parameters were used as in the bandgap calculations. The absorption spectrum can be derived from the imaginary part of the complex dielectric constant, which was calculated from the susceptibility tensor that characterizes the polarization level of the material subjects to an electric field. Previous studies described in detail the procedures for calculating the absorption coefficient.[27,28] The calculated anisotropic optical absorptions of both crystal phases are shown in Fig. 5. It is shown that for α-Ga_2O_3, the optical absorption spectra in the x- and y-directions are exactly overlapping each other; however, the absorption coefficient in the z-direction is very much different, especially at the wavelength around 150 nm, where there is a peak absorption exceeding 40 μm^{-1}. For the β-Ga_2O_3, the optical absorption coefficients exhibit strong anisotropicity in three directions. On comparing these two types of materials, the absorption spectrum of the β-Ga_2O_3 is much wider, corresponding to its narrower bandgap.

More DFT simulation has been conducted to calculate the formation energies for the unit cell of both α-Ga_2O_3 and β-Ga_2O_3. The same computational procedure, as previously described, was used, and the equation $E_f = E_{Ga_2O_3}/n - (2 \cdot E_{Ga} + 3 \cdot E_O)$ was adopted for both types of materials, where E_f is the formation energy of

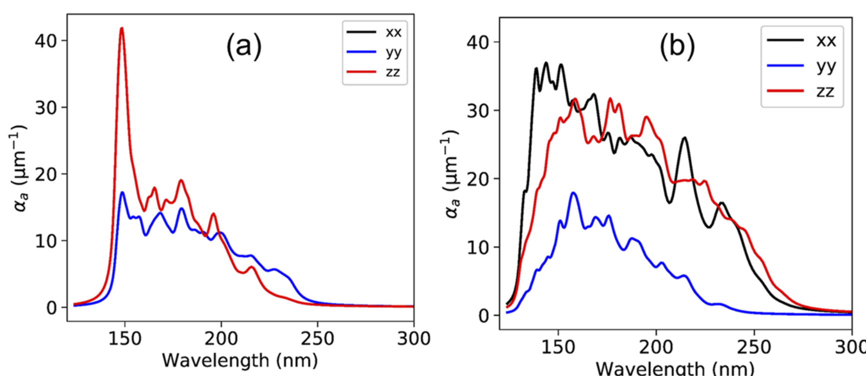

FIG. 5. Simulated optical absorption of α-Ga_2O_3 (a) and β-Ga_2O_3 (b).

© Author(s) 2022

a unit cell containing 2 Ga and 3 O, and n is the number of unit cells in a supercell. E_{Ga}, E_O, and $E_{Ga_2O_3}$ are the total energies of Ga, O, and Ga_2O_3 supercell, respectively. It is calculated that E_f of alpha and beta types are −18.226 and −18.159 eV, respectively. The E_f value of α-Ga_2O_3 is 67 meV lower than that of β-Ga_2O_3, indicating that extra energy is required to convert α- to β-phase. This coincides with the fact that α-phase can be converted to beta at a high temperature.

CONCLUSION

This study aimed to find the possibility of using MW radiation power to induce Ga_2O_3 phase change. It is found that increasing the MW treatment time results in stronger β-phase character Ga_2O_3. The XRD results show that the intensity of two peaks at ~64.4° and ~77.4° increased with an increase in the MW treatment time, which are related to forbidden (512) and (421) plane reflections, respectively. This confirms that the Ga_2O_3 phase changes from room temperature PVD deposited α-Ga_2O_3 to β- Ga_2O_3. Moreover, transmittance measurements of the as-grown Ga_2O_3 and MW treated Ga_2O_3 thin films show that treated samples have slightly narrower bandgaps at about 4.8 and 4.75 eV for 5 and 20 min MW treatments, respectively, compared with the Ga_2O_3 grown by the PVD (4.9 eV), and the β- Ga_2O_3 prepared by the PVD together with post annealing process using furnace at 700 °C demonstrating a 4.65 eV bandgap. SEM imaging of the samples before and after 5 and 20 min MW treatments shows that increasing the MW treatment time leads to particle agglomeration, annealing, and sintering, hence improving the crystallinity. Further theoretical study using DFT has been conducted to verify the experiments, which shows that the bandgap of the β- Ga_2O_3 is narrower than that of the α-Ga_2O_3. The optical absorption of the β-Ga_2O_3 has much stronger anisotropicity. The reported experiment paves a way for low-cost fabrication of β-Ga_2O_3.

ACKNOWLEDGMENTS:

The authors acknowledge the support from the European Regional Development Fund (ERDF) for funding the Solar Photovoltaic Academic Research Consortium (SPARC II), and the EPSRC Project (Grant No. EP/T019085/1).

AUTHOR DECLARATIONS

Conflict of Interest

The authors have no conflicts to disclose.

Author Contributions

Nafiseh Badiei: Conceptualization (equal); Data curation (equal); Formal analysis (equal); Investigation (equal); Methodology (equal); Validation (equal); Visualization (equal); Writing – original draft (equal); Writing – review & editing (equal). **Afshin Tarat**: Conceptualization (equal); Formal analysis (equal); Investigation (equal); Methodology (equal); Writing – original draft (equal); Writing – review & editing (equal). **Lijie Li**: Conceptualization (equal); Data curation (equal); Formal analysis (equal); Funding acquisition (equal); Investigation (equal); Methodology (equal); Project administration (equal); Resources (equal); Software (equal); Supervision (equal); Validation (equal); Visualization (equal); Writing – original draft (equal); Writing – review & editing (equal).

DATA AVAILABILITY

The data that support the findings of this study are available from the corresponding author upon reasonable request.

REFERENCES

[1]S. J. Pearton, J. Yang, P. H. Cary, F. Ren, J. Kim, M. J. Tadjer, and M. A. Mastro, Appl. Phys. Rev. **5**(1), 011301 (2018).
[2]H. Y. Playford, A. C. Hannon, E. R. Barney, and R. I. Walton, Chem.-Eur. J. **19**(8), 2803–2813 (2013).
[3]A. J. Green, J. Speck, G. Xing, P. Moens, F. Allerstam, K. Gumaelius, T. Neyer, A. Arias-Purdue, V. Mehrotra, A. Kuramata, K. Sasaki, S. Watanabe, K. Koshi, J. Blevins, O. Bierwagen, S. Krishnamoorthy, K. Leedy, A. R. Arehart, A. T. Neal, S. Mou, S. A. Ringel, A. Kumar, A. Sharma, K. Ghosh, U. Singisetti, W. Li, K. Chabak, K. Liddy, A. Islam, S. Rajan, S. Graham, S. Choi, Z. Cheng, and M. Higashiwaki, APL Mater. **10**(2), 029201 (2022).
[4]C.-H. Lin and C.-T. Lee, J. Lumin. **224**, 117326 (2020).
[5]D. H. Vieira, N. Badiei, J. E. Evans, N. Alves, J. Kettle, and L. Li, IEEE Trans. Electron Devices **67**(11), 4947–4952 (2020).
[6]L. Dong, T. Pang, J. Yu, Y. Wang, W. Zhu, H. Zheng, J. Yu, R. Jia, and Z. Chen, J. Mater. Chem. C **7**(45), 14205–14211 (2019).
[7]M. H. Wong, K. Goto, H. Murakami, Y. Kumagai, and M. Higashiwaki, IEEE Electron Device Lett. **40**(3), 431–434 (2019).
[8]K. D. Chabak, K. D. Leedy, A. J. Green, S. Mou, A. T. Neal, T. Asel, E. R. Heller, N. S. Hendricks, K. Liddy, A. Crespo, N. C. Miller, M. T. Lindquist, N. A. Moser, R. C. Fitch, D. E. Walker, D. L. Dorsey, and G. H. Jessen, Semicond. Sci. Technol. **35**(1), 013002 (2019).
[9]Y. Liao, Z. Zhang, Z. Gao, Q. Qian, and M. Hua, ACS Appl. Mater. Interfaces **12** (27), 30659–30669 (2020).
[10]L. Li, Carbon Trends **7**, 100153 (2022).
[11]Y. Yao, S. Okur, L. A. M. Lyle, G. S. Tompa, T. Salagaj, N. Sbrockey, R. F. Davis, and L. M. Porter, Mater. Res. Lett. **6**(5), 268–275 (2018).
[12]J. Lee, H. Kim, L. Gautam, K. He, X. Hu, V. P. Dravid, and M. Razeghi, Photonics **8**(1), 17 (2021).
[13]R. Roy, V. G. Hill, and E. F. Osborn, J. Am. Chem. Soc. **74**(3), 719–722 (1952).
[14]B. Choi, B. Allabergenov, H.-K. Lyu, and S. E. Lee, Appl. Phys. Express **11**(6), 061105 (2018).
[15]C. A. Deshmane, J. B. Jasinski, and M. A. Carreon, Microporous Mesoporous Mater. **130**(1), 97–102 (2010).
[16]L. S. Reddy, Y. H. Ko, and J. S. Yu, Nanoscale Res. Lett. **10**(1), 364 (2015).
[17]P. Jaiswal, U. Ul Muazzam, A. S. Pratiyush, N. Mohan, S. Raghavan, R. Muralidharan, S. A. Shivashankar, and D. N. Nath, Appl. Phys. Lett. **112**(2), 021105 (2018).
[18]S. Horikoshi, T. Watanabe, A. Narita, Y. Suzuki, and N. Serpone, Sci. Rep. **8**(1), 5151 (2018).
[19]C. Leonelli and T. J. Mason, Chem. Eng. Process. **49**(9), 885–900 (2010).
[20]G. Pozina, M. Forsberg, M. A. Kaliteevski, and C. Hemmingsson, Sci. Rep. **7**(1), 42132 (2017).
[21]J. Huang, B. Li, Y. Ma, K. Tang, H. Huang, Y. Hu, T. Zou, and L. Wang, IOP Conf. Ser.: Mater. Sci. Eng. **362**, 012003 (2018).
[22]Y. J. Lee, M. A. Schweitz, J. M. Oh, and S. M. Koo, Materials **13**(2), 434 (2020).
[23]L. Li, AIP Adv. **11**(6), 065111 (2021).
[24]A. Segura, L. Artús, R. Cuscó, R. Goldhahn, and M. Feneberg, Phys. Rev. Mater. **1**(2), 024604 (2017).
[25]E. Ahmadi and Y. Oshima, J. Appl. Phys. **126**(16), 160901 (2019).
[26]J. W. Roberts, P. R. Chalker, B. Ding, R. A. Oliver, J. T. Gibbon, L. A. H. Jones, V. R. Dhanak, L. J. Phillips, J. D. Major, and F. C.-P. Massabuau, J. Cryst. Growth **528**, 125254 (2019).
[27]X. Cai, S. Deng, L. Li, and L. Hao, J. Comput. Electron. **19**(3), 910–916 (2020).
[28]S. Deng, Y. Zhang, and L. Li, Appl. Surf. Sci. **476**, 308–316 (2019).

© Author(s) 2022